
This is an electronic reprint of the original article.
This reprint may differ from the original in pagination and typographic detail.

Nekoueian, Khadijeh; Kontturi, Katri S; Meinander, Kristoffer; Quliyeva, Ulviyya; Kousar, Ayesha; Durairaj, Vasuki; Tammelin, Tekla; Laurila, Tomi

Advanced Nanocellulose-Based Electrochemical Sensor for Tetracycline Monitoring

Published in:
Electrochimica Acta

DOI:
[10.1016/j.electacta.2024.144639](https://doi.org/10.1016/j.electacta.2024.144639)

Published: 01/10/2024

Document Version
Publisher's PDF, also known as Version of record

Published under the following license:
CC BY

Please cite the original version:
Nekoueian, K., Kontturi, K. S., Meinander, K., Quliyeva, U., Kousar, A., Durairaj, V., Tammelin, T., & Laurila, T. (2024). Advanced Nanocellulose-Based Electrochemical Sensor for Tetracycline Monitoring. *Electrochimica Acta*, 500, Article 144639. <https://doi.org/10.1016/j.electacta.2024.144639>

This material is protected by copyright and other intellectual property rights, and duplication or sale of all or part of any of the repository collections is not permitted, except that material may be duplicated by you for your research use or educational purposes in electronic or print form. You must obtain permission for any other use. Electronic or print copies may not be offered, whether for sale or otherwise to anyone who is not an authorised user.



Advanced nanocellulose-based electrochemical sensor for tetracycline monitoring

Khadijeh Nekoueian^{a,*}, Katri S. Kontturi^b, Kristoffer Meinander^c, Ulviyya Quliyeva^a, Ayesha Kousar^a, Vasuki Durairaj^b, Tekla Tammelin^b, Tomi Laurila^{a,d,*}

^a Department of Electrical Engineering and Automation, School of Electrical Engineering, Aalto University, PO Box 13500, 00076 Aalto, Finland

^b Biomass Processing and Products, VTT Technical Research Centre of Finland, PO Box 1000, FI-02044 Espoo, Finland

^c Department of Bioproducts and Biosystems, School of Chemical Engineering, Aalto University, PO Box 16300, 00076 Aalto, Finland

^d Department of Chemistry and Materials Science, School of Chemical Engineering, Aalto University, PO Box 16100, 00076 Aalto, Finland

ARTICLE INFO

Keywords:

TEMPO-oxidized cellulose nanofibers
Polyethyleneimine
Single-walled carbon nanotube networks
Electrochemical sensors
Voltammetric determination
Tetracycline

ABSTRACT

Antibiotics play a pivotal role in healthcare and agriculture, but their overuse and environmental presence pose critical challenges. Developing sustainable and effective detection methodologies is crucial to mitigating antibiotic resistance and environmental contamination. This study presents a cellulosic polymer-based electrochemical sensor by integrating TEMPO-oxidized cellulose nanofibers-polyethyleneimine hybrids (TOCNFs-PEI) with single-walled carbon nanotube networks (SWCNTs). Our research focuses on (i) conducting physico-chemical and electrochemical studies of multifunctional SWCNT/TOCNFs-PEI architectures, (ii) elucidating the relationships between the material's properties and their electrochemical performance, and (iii) assessing its performance in detecting tetracycline concentrations in both controlled and more complex matrices (treated wastewater effluents). The limits of detection were evaluated to be $0.180 \mu\text{mol L}^{-1}$ (at the potential of 0.85 V) and $0.112 \mu\text{mol L}^{-1}$ (at the potential of 0.65 V) in phosphate-buffered saline solution, and $2.46 \mu\text{mol L}^{-1}$ (at the potential of 0.82 V) and $1.5 \mu\text{mol L}^{-1}$ (at the potential of 0.65 V) in the undiluted membrane bioreactor effluent sample, respectively. Further, the designed cellulosic polymer-based sensing architecture is compatible with large-scale production, paving the way for a new era of green, versatile sensing devices. These developments will significantly contribute to global efforts to alleviate antibiotic resistance and environmental contamination.

1. Introduction

Antibiotics are essential for treating human and animal infections, but their misuse and overuse as growth promoters in livestock and aquaculture lead to their continuous introduction into the environment [1,2]. The most common antibiotics found in wastewater samples are sulfonamides, tetracyclines, lincomycin, ofloxacin, and trimethoprim [3,4]. However, their distribution varies worldwide [5]. While wastewater treatment plants (WWTPs) are effective in eliminating a wide range of waterborne contaminants, certain antibiotics may be persisted or be released into water sources during these treatment processes [5-7]. Membrane bioreactors (MBRs) are known as advanced wastewater treatment technologies that combine biological treatment processes with membrane filtration [7]. Even though MBRs are good at removing various pharmaceutical compounds from wastewater, the fact that antibiotics are still present in the treated wastewater is a problem [8,9].

The efficiency of MBRs in the removal of antibiotics is affected by different factors such as the size and the lifespan of the membranes, and the buildup of biological material in the system (biofouling) [8,10]. Tetracycline (TC) is one of the antibiotics that was primarily quantified in both the liquid and sludge fractions of MBR in WWTPs [11]. Routine monitoring of safe antibiotic concentrations including TC in treated effluents is vital to ensure compliance with regulatory standards and mitigate long-term effects like antibiotic resistance and environmental contamination [5,11-15]. Unlike conventional analytical methods, electrochemical techniques offer a reliable technique for sensitive and cost-effective detection of TC [16-18]. Electrochemical methods excel at detecting trace amounts of analytes in complex matrices, offer automation, and allow simultaneous detection of multiple compounds, thus enabling rapid real-time monitoring [19,20]. The demand for green detection technologies has driven interest in cellulose-based nanomaterials for the design of smart materials and electrochemical sensors

* Corresponding authors.

E-mail addresses: Khadijeh.Nekoueian@Aalto.Fi (K. Nekoueian), Tomi.Laurila@Aalto.Fi (T. Laurila).

<https://doi.org/10.1016/j.electacta.2024.144639>

Received 26 March 2024; Received in revised form 26 June 2024; Accepted 28 June 2024

Available online 29 June 2024

0013-4686/© 2024 The Authors. Published by Elsevier Ltd. This is an open access article under the CC BY license (<http://creativecommons.org/licenses/by/4.0/>).

[21]. Cellulose, abundant and renewable, presents an alternative to fossil-derived materials [22]. The natural properties of cellulose and its derivatives, like the abundance of hydroxyl groups for chemical modifications, besides its controlled porosity and high surface-to-volume ratio, make it attractive for sensor design [22,23]. However, cellulose's non-conductive nature has limited its usage in the electrochemical sensors [24]. To address this issue, researchers have modified cellulose-based materials with various nanomaterials (such as conducting polymers, carbon nanostructures, and metal nanostructures) and different functional groups to expand their applications [24,25]. Polyethyleneimine (PEI) is a positively charged polymer known for its electrical conductivity and chemical and physical stability [26,27]. It offers advantages such as low toxicity, biocompatibility, low cost, recyclability, and the ability to form thin films [26,28,29]. The high number of active amino groups in the PEI structure makes it a suitable candidate for reacting with other materials with carboxyl groups [30] and the design of electrochemical (bio)sensors [28,30]. TEMPO-oxidized cellulose nanofibers (TOCNFs) featuring activated carboxylate surface groups (COO^-) demonstrate effective interaction with active amino groups ($-\text{NH}_2^+$ and $-\text{NH}_3^+$) of PEI [31]. This interaction results in the formation of the TOCNFs-PEI through a combination of hydrogen bonding and electrostatic interactions [32,33]. The TOCNFs-PEI, having a cellulose nanofiber structure with carboxyl and amino groups, serve as active adsorption sites [34]. These sites facilitate the extraction of substances like cationic heavy metals, organic molecules, and biological compounds through electrostatic attraction and coordination interactions [31,34,35]. TOCNFs-PEI was utilized in the eco-friendly design of rapid colourimetric sensors for naked-eye detection of fluoride anions, as reported by Melone et al. [36] and Riva's group [37]. Recently, Takahashi and his team introduced voltammetric sensors based on cellulose for detecting diol and polyol compounds, including 3,4-dihydroxyphenylalanine (L-DOPA) [38]. In the first step, they coat a gold electrode with carboxymethylcellulose and PEI films with a layer-by-layer technique. Subsequently, they treated the electrode with Alizarin red S, providing redox activity for sensing polyol compounds with tunable electrochemical properties in the presence of phenylboronic acid (PBA) [38]. The research group later improved the system by directly grafting PBA onto the PEI for enhanced sensing performance [39]. In another noteworthy example of the importance of nanocellulose-PEI composites in sensing, Zhang and colleagues reported synthesizing gold nanoparticle-bacteria cellulose nanofiber (BNC) composites. Here, PEI served as both a reducing agent for gold nanoparticle (GP) synthesis and a linking agent between GPs and BNC. The resulting nanocomposite served as a support for horseradish peroxidase, leading to a biosensor with a detection limit below $1 \mu\text{mol L}^{-1}$. Additionally, the same support demonstrated utility for immobilizing other enzymes for heterogeneous catalysis [40]. Furthermore, Terasawa et al. demonstrated that combining TOCNFs with SWCNTs and ionic liquids (CNFs/SWCNTs/ILs) created highly entangled networks. These networks are suitable for designing gel electrodes and electrolytes for energy-conversion devices [41,42].

In this study, we employed an optimized ratio of TOCNF-PEI suspension to modify the surface of SWCNTs, creating SWCNTs/TOCNF-PEI for the development of an electrochemical sensor tailored for TC monitoring. Our research aims to (i) conduct comprehensive physicochemical and electrochemical studies of SWCNT/TOCNF-PEI architectures, (ii) elucidate the intricate relationships between SWCNTs/TOCNF-PEI properties and their electrochemical performance, and (iii) evaluate sensor efficacy in detecting TC concentrations within controlled environments such as phosphate-buffered saline solution (PBS) and undiluted MBR effluent samples. Leveraging the inherent electrical conductivity and mechanical strength of SWCNTs (as extensively studied within our research group [43,44]), the SWCNTs networks serve as a reliable sensing support. Notably, this setup eliminates the need for modifying conventional electrodes, streamlining the sensor fabrication process. The eco-friendly preparation of TOCNF-PEI reduces

hazardous chemical usage and energy consumption, aligning with sustainability goals and lowering the environmental impact of electrode material production. The sustainable nature of the SWCNTs/TOCNF-PEI setup, along with its compatibility with large-scale sensor strip production [43,45,46], positions it as a promising candidate for the development of next-generation "green" sensing devices, poised to make significant contributions across various industries.

2. Experimental

2.1. Reagents

TOCNFs were obtained through TEMPO-mediated oxidation of bleached birch pulp, as described by Saito et al. [25,47]. The TOCNFs gel (with a dry content of around 1%) had a degree of carboxyl group (COO^-) substitution of 0.9 mmol/g. The PEI solution (a branched polymer, average $M_n \sim 60,000$ by GPC, average $M_w \sim 750,000$ by LS, 50 wt.% in H_2O), hexaammineruthenium (III) chloride, and tetracycline hydrochloride were supplied from Sigma-Aldrich. All other chemicals were of analytical reagent grade and were obtained from Merck. All aqueous solutions and suspensions were prepared by using doubly distilled deionized water. The PBS solution (1 L) was provided by mixing 8 g of NaCl, 0.2 g of KCl, 1.44 g of Na_2HPO_4 , and 0.24 g of KH_2PO_4 with distilled water. The pH of the solution was carefully adjusted and maintained at 7.4 using either a 1 mol L^{-1} HCl solution or a 1 mol L^{-1} NaOH solution.

2.2. Preparation of TOCNF-PEI

The TOCNF gel (1.0 wt%) was diluted to a concentration of 0.1 wt% through sonication in deionized water using a Qsonica Q500 tip sonicator with a 2 mm probe. Sonication was conducted in an ice bath with the following parameters: a frequency of 20 kHz, a power output of 30 W, and a pulsing mode of 5 s on, followed by 1 s off, for 10 min. Afterwards, the 0.1 wt% TOCNF suspension and a 0.1 wt% PEI solution were mixed at different ratios (w/w), i.e., 3:1, 2:1, 1:1, and 1:2, and stirred magnetically for 24 h at room temperature. The ratio of 2:1 was used in sample preparation for further studies. The resulting TOCNF-PEI was stored in the fridge for future use [32,33].

2.3. SWCNTs fabrication

SWCNTs were obtained from Canatu Oy and were prepared using floating catalyst chemical vapour deposition (CVD) in a laminar flow reactor. In this method, an iron-containing precursor was thermally decomposed in a carbon monoxide environment to produce iron nanoparticles. In a quartz laminar flow reactor, the iron nanoparticles promote the breakdown of carbon monoxide, causing SWCNT to form and develop in the gas phase. SWCNT networks were formed with diameters of $17 \times 25.5 \text{ cm}^2$, and then SWCNTs were collected on A4-sized nitrocellulose filters, and bundles were created in the gas phase. Comprehensive fabrication details are provided in Kaskela et al. [46], Moisala et al. [48]. These SWCNT networks are compatible with the large-scale production of sensor strips. Our previous works provided a comprehensive account of the preparation and physicochemical as well as electrochemical characterization of SWCNT networks [44,49].

2.4. Electrode preparation

SWCNT networks were cut from nitrocellulose filter paper and transferred onto a glass slide ($1 \times 2 \text{ cm}^2$) by pressing. The filter paper was then peeled off, and the adhered SWCNT network was densified with ethanol and left to dry. Silver contact pads were applied using conductive silver paint to the glass slide and allowed to dry for at least one hour. A piece of conductive copper tape was attached to enhance conductivity and connect to a copper body. A protective layer of

polytetrafluoroethylene (PTFE) tape with a 3 mm diameter hole was applied to sandwich the SWCNT/glass slide and copper body [43,46]. This ensured that only the designated electrode surface area was exposed to the analyte, preventing interference from the surrounding environment. Subsequently, a 14 μL drop of TOCNF-PEI suspension was drop cast onto the surface of SWCNT electrodes and allowed to dry for 1 h in an incubator set at 70 °C. A detailed description of the preparation of SWCNT-based electrodes is available in the work by Leppänen et al. [49] and Wester et al. as illustrated in Scheme S1 [43,50].

2.5. Instruments and methods

Cyclic voltammetry (CV) and differential pulse voltammetry (DPV) measurements were conducted using a Gamry potentiostat (Reference 600) coupling with a conventional three-electrode system including a working electrode, a saturated Ag/AgCl reference electrode, and a Pt wire as the counter electrode. A silver wire coated with AgCl was used as a reference electrode for conducting the measurements in the MBR effluent sample. Voltammetric experiments were carried out in PBS (pH 7.4, 0.1 M). All solutions were deoxygenated by purging them with pure nitrogen for 30 min before conducting measurements. The electrochemical measurements were conducted at SWCNT and SWCNT/TOCNF-PEI electrodes after immersion of them for 30 min in a blank solution and subsequent CV (25 cycles) in PBS (pH 7.4) to stabilize the response signal (Fig. S1). In the present study, we employed the DPV method that consisted of two steps: (i) immersing the electrode in the sample solution, which contained TC and PBS (the background electrolyte), for an optimal period, and (ii) running DPV in the same solution. There was no electro-accumulation phase before operating the DPV. Furthermore, the effect of pulse size, step size, and pulse time on the DPV peak signal was investigated to optimize this method for detecting TC. The highest peak current was achieved with a pulse size E of 75 mV, a step size of 5 mV, a pulse time of 0.05 s, and a sample period of 0.2 s; therefore, these were chosen as the optimal parameters and were used for all the DPV measurements.

Morphological and structural characterization of the SWCNT and SWCNT/TOCNF-PEI electrodes were studied by scanning electron microscopy (SEM) (Zeiss Sigma VP). A Micro-Raman spectroscope (WITec Alpha 300 RA+), equipped with an optical microscope, was utilized for Raman spectroscopy, employing a laser excitation wavelength of 532 nm with a 50 \times objective lens. Data analysis was conducted using WITec Suite 5.1 software. Spectra fitting was performed with one Lorentzian peak for the D band and two Lorentzian peaks for the G band [45]. The Jupiter XR atomic force microscope (AFM) was employed to analyse surface topography in air, and the Gwyddion program was used for data visualization and analysis.

The chemical structure of SWCNT/TOCNFs-PEI was studied via Fourier transform infrared (FTIR) spectroscopy (Bruker Alpha II FTIR spectrometer) in attenuated total reflection (ATR) mode. X-ray photoelectron spectroscopy (XPS) was used to examine the elemental composition of the samples and detect differences in the C 1s, N 1s, and O 1s spectra. The measurements were performed with a Kratos AXIS Ultra DLD X-ray photoelectron spectrometer using a monochromated Al K_{α} X-ray source (1486.7 eV) run at 100 W. A pass energy of 80 eV and a step size of 1.0 eV were used for the survey spectra, while a pass energy of 20 eV and a step size of 0.1 eV were used for the high-resolution spectra. Photoelectrons were collected at a 90° take-off angle under ultra-high vacuum conditions, with a base pressure typically below 1×10^{-9} Torr. The diameter of the beam spot from the X-ray was 1 mm, and the area of analysis for these measurements was 300 μm x 700 μm . All spectra were charge-corrected relative to an energy of C—C bonding at 284.8 eV. The CasaXPS software was used for the analysis of XPS results. Glass slides were used as a substrate of samples for Raman, AFM, FTIR and XPS studies.

The sign of the overall electrostatic charge of TOCNF-PEI complex in different TOCNF:PEI component ratios were studied visually and

spectrophotometrically (PerkinElmer Lambda 900 UV/Vis spectrophotometer, PerkinElmer, USA) utilising a cationic indicator colour and polyelectrolyte titration. 10 mL of 0.01 w-% TOCNF suspension with 1 mL of 0.01 w-% ortho-toluidine blue (OTB) indicator was titrated with 10 μL additions of 0.01 w-% PEI solution. In the aqueous suspension, the cationic OTB is initially bound by the anionic TOCNF until the quantity of added cationic PEI is adequate to occupy all available anionic charges of TOCNF upon formation of TOCNF-PEI complex, replacing all the previously bound OTB and releasing it into the suspension. The release of the OTB, indicating the point of charge neutrality of the complex, is indicated by the suspension colour change from purple to blue. This was observed both visually and by spectroscopically quantifying the intensity of the absorbance signals at 628 nm taking over the intensity at \sim 510 nm (Fig. S2).

3. Results and discussion

3.1. Structural characterization

The surface morphology and topography of SWCNT and SWCNT/TOCNF-PEI were studied using SEM and AFM. Fig. 1A and B show these materials' SEM and AFM images, along with their corresponding roughness profiles. Analysing the surface topography and calculating the root mean square roughness (R_q) indicated the attachment of the TOCNF-PEI layer on the SWCNT. This is evident from the decrease in R_q from 5.14 ± 0.65 nm for SWCNT to 2.988 ± 0.87 nm for SWCNT/TOCNF-PEI. The R_q values were obtained by averaging multiple vertical and horizontal line scans over a $5 \times 5 \mu\text{m}^2$ area using Gwyddion software.

Raman spectroscopy was used to study the structural and electronic properties of SWCNT and the SWCNT/TOCNF-PEI (Fig. 2A). The Raman spectrum of SWCNT exhibited a multiple peak G mode around 1594 cm^{-1} and a weak D band around 1340 cm^{-1} . The D band rises due to defects or disorder in the carbon structure, while the G band is associated with the stretching motion of pairs of sp^2 carbon atoms in the hexagonal lattice of the nanotube. The low intensity of the D band indicated a small number of defects and an insignificant amount of amorphous carbon in SWCNT [43,51]. The ratio of the intensity of these two bands (I_D/I_G ratio) is used to display the number of defects in carbon-based materials [52]. The I_D/I_G values were determined to be 0.049 ± 0.01 for SWCNT, exhibiting a slight decrease to 0.037 ± 0.05 at SWCNT/TOCNF-PEI. These assessments were conducted using the Lorentzian function fit method, as outlined in the literature [52]. Importantly, these results align consistently with earlier investigations carried out within our research group [45]. It can be deduced that SWCNT and SWCNT/TOCNF-PEI possess comparable structural and electronic properties in terms of defects and disorders in their carbon structure, a notion that was confirmed in further electrochemical studies.

Fig. 2B displays the FTIR spectrum of the SWCNT, SWCNT/TOCNF, SWCNT/PEI, and SWCNT/TOCNF-PEI. Two significant absorption bands were observed in the SWCNT/TOCNF sample at 3294 cm^{-1} assigned to the stretching vibration of O—H, and at 1637 cm^{-1} allocated to the stretching vibrations of COO^- [53,54]. The absence of the COO^- band in the SWCNT/TOCNF-PEI spectrum may be attributed to the efficient interaction between the carboxyl groups of TOCNF and the amino groups of PEI, leading to the formation of amide bonds (N—C=O), as reported by [55,56]. This is additionally supported by the XPS results (refer to below). Moreover, the emergence of new spectral peaks at 1572 cm^{-1} and 1336 cm^{-1} , indicative of N—H in-plane and C—N bond stretching (Fig. S3), respectively, provides further evidence of the presence of the amide functional group [57,58].

The XPS measurements provided additional evidence of the formation of the TOCNF-PEI (Fig. 3). Table 1 gives the relative concentrations of different elements in the surface layers of SWCNT, SWCNT/TOCNF, SWCNT/PEI, and SWCNT/TOCNF-PEI. The carbon content is fairly similar for all samples, with the biggest differences appearing in the

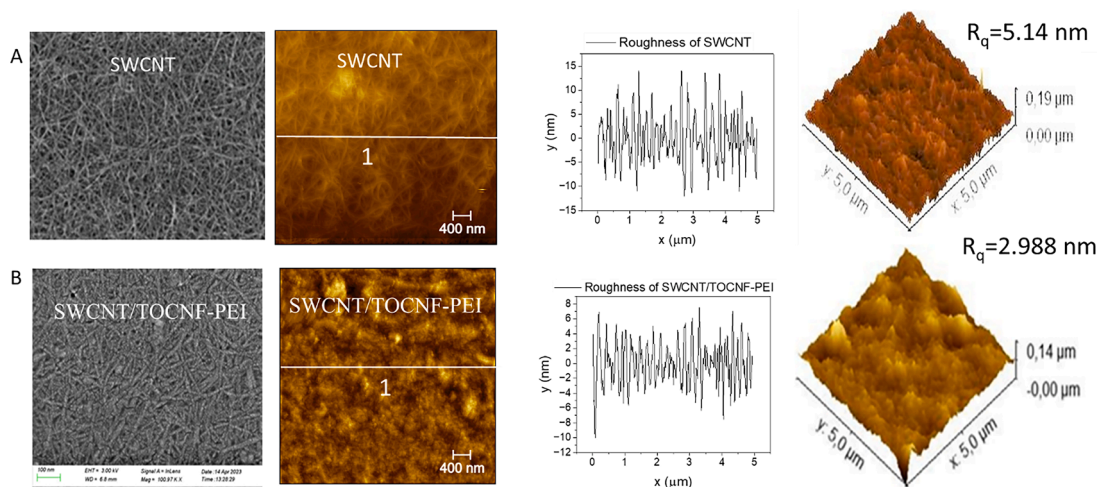


Fig. 1. SEM, AFM images and corresponding roughness profiles of the SWCNT (A); and the SWCNT/TOCNF-PEI (B). The roughness profiles are derived from the displayed line 1. R_q evaluated from the average of 40 vertical and horizontal line scans over a $5 \times 5 \mu\text{m}^2$ scan area.

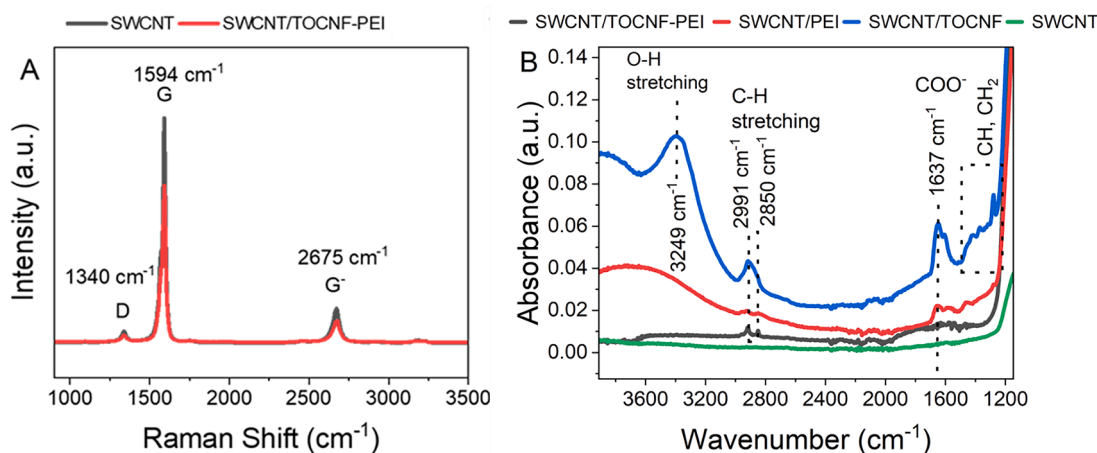


Fig. 2. The Raman spectrum of the SWCNT (black line) and the SWCNT/TOCNF-PEI (red line) (A); the FTIR spectrum of the SWCNT (green line), the SWCNT/TOCNF (blue line), the SWCNT/PEI (red line) and the SWCNT/TOCNF-PEI (black line) (B).

nitrogen and oxygen contents. Trace amounts of sodium and chlorine were also detected in some samples (Table 1). As expected, increased nitrogen content can be seen for the PEI-containing samples, while oxygen content was higher for samples containing TOCNF. The O 1s peak in SWCNT/TOCNF-PEI indicated a lower concentration of oxygen compared to the SWCNT/TOCNF sample (Fig. 3A). Nevertheless, the N 1s XPS spectrum demonstrated the emergence of nitrogen (N) into the structure of SWCNT/TOCNF-PEI, consistent with findings in previously reported PEI-modified materials [59,60].

This change in the N and O content in SWCNT/TOCNF-PEI could be attributed to a chemical reaction involving the carboxyl groups ($-\text{COOH}$) of TOCNF and the amino groups of PEI, leading to the formation of amide bonds ($\text{N}-\text{C}=\text{O}$). In the N 1s spectrum of TOCNF-PEI (Fig. 3B), three distinct peaks were observed at 401.1, 400.1, and 399.3 eV, corresponding to amide (9.8%), tertiary amine (23.6%), and secondary amine (60.5%), respectively [61]. Furthermore, the relative ratio between the amide peak and the secondary amine peak in the XPS spectra increased from approximately 0.11 in SWCNT/PEI to about 0.16 in SWCNT/TOCNF-PEI. This suggests a higher prevalence of amide bond formation in SWCNT/TOCNF-PEI compared to SWCNT/PEI, indicating the possibility of amide bond formation between the readily electrostatically bound TOCNF and PEI upon the drying of the drop-cast samples at elevated temperatures. A minor component in the N 1s spectra

was detected at a lower energy, around 398.1 eV, possibly indicating the presence of primary amines. Additionally, two higher energy components were identified at approximately 406.4 eV and 407.8 eV, attributed to nitrite and nitrate contamination in the SWCNT. These contaminations diminished in other samples due to surface modification with PEI and TOCNF-PEI.

The O 1s and N 1s XPS spectra of SWCNT/TOCNF-PEI were studied after incubation with $100 \mu\text{mol L}^{-1}$ TC in 0.1 mol L^{-1} PBS pH 7.4 and subsequent rinsing with the deionized water (Fig. 3 and Table S1). Some small changes occurred in both the total nitrogen content and the ratio between the amide peak and the secondary amine peak, which reached approximately 0.20. This increase suggests the adherence of TC molecules containing amide groups (CONH_2), dimethylamino groups ($\text{N}(\text{CH}_3)_2$), and phenolic hydroxyl groups, to SWCNT/TOCNF-PEI, as shown in Table S1.

3.2. Electrochemical characterization of the SWCNT/TOCNF-PEI

The basic electrochemical performance of both the SWCNT and SWCNT/TOCNF-PEI electrodes was evaluated using CV. The study was conducted in the presence of a 1 mmol L^{-1} $\text{Ru}(\text{NH}_3)_6^{2+/3+}$ solution within a 1 mol L^{-1} KCl solution, utilizing it as an outer-sphere redox probe (OSR). The OSR interacts with the electrodes without inducing

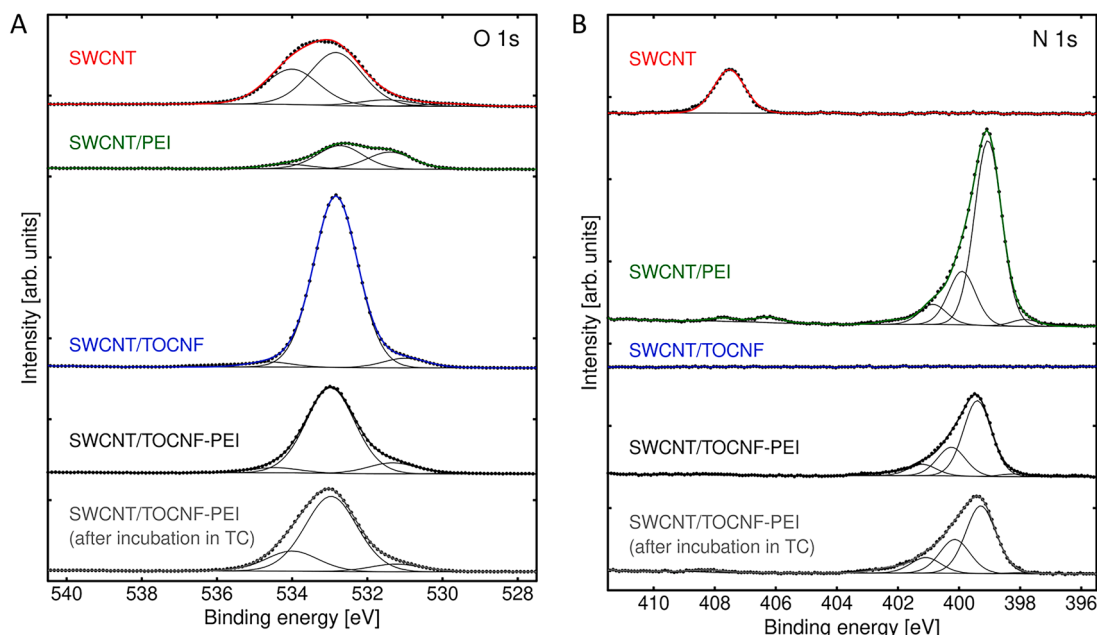


Fig. 3. O 1s (A) and N 1s (B) XPS spectra of SWCNT, SWCNT/TOCNF, SWCNT/PEI, SWCNT/TOCNF-PEI and SWCNT/TOCNF-PEI after incubation in TC solution.

Table 1

Relative concentrations of elements in the samples. Values are given in units of atomic percentage. It should be noted that approximately 0.5% of the total composition is attributed to trace amounts of sodium and chlorine.

Sample	C 1s %	N 1s %	O 1s %	Cl 2p %	Na 1s %
SWCNT	70.3 ± 1.24	4.01 ± 0.33	25.5 ± 0.91	0.00	0.18 ± 0.01
PEI/SWCNT	68.4 ± 0.09	20.8 ± 0.07	10.4 ± 0.20	0.25 ± 0.04	0.00
TOCNF/SWCNT	61.5 ± 0.12	0.00 ± 0.00	37.7 ± 0.16	0.00	0.71 ± 0.07
TOCNF/PEI/SWCNT	66.8 ± 0.76	9.38 ± 0.13	23.4 ± 0.71	0.09 ± 0.06	0.26 ± 0.03
TC/TOCNF/PEI/SWCNT	64.5 ± 0.34	9.92 ± 0.08	25.3 ± 0.28	0.19 ± 0.04	0.00

any chemical or electrocatalytic reactions, making it a valuable tool for assessing the electronic structure of the electrode without complications from surface chemistry. Both the SWCNT and SWCNT/TOCNF-PEI electrodes exhibited a strong redox signal in the Ru (NH₃)₆^{2+/3+} solution. The anodic peak current (*I*_{pa}) and cathodic peak current (*I*_{pc}) values for SWCNT were 21.07 ± 0.07 μA and -24.16 ± 0.12 μA, respectively. Upon surface modification with TOCNF-PEI, these values increased to *I*_{pa} (31.51 ± 1.12 μA) and *I*_{pc} (-36.1 ± 2.3 μA) for SWCNT/TOCNF-PEI. The observed *I*_{pa}/*I*_{pc} ratio smaller than 1 (as shown in Table 2) indicates weak product adsorption, likely due to stronger electrostatic interactions between the oxidized form of Ru (which carries

Table 2

The comparison of the parameters obtained from the CV for SWCNT and the SWCNT/TOCNF-PEI electrodes in the presence of 1 mmol L⁻¹ Ru (NH₃)₆^{2+/3+} in 1 mol L⁻¹ KCl solution (*N* = 3). Nicholson's method was used to evaluate *k*⁰, while the Randles-Ševčík equation was used to calculate *A*_{eff} [65]. The diffusion coefficients required to evaluate these parameters were obtained from reference [66].

Electrode	<i>I</i> _{pa} (μA)	<i>I</i> _{pc} (μA)	<i>I</i> _{pa} / <i>I</i> _{pc}	<i>E</i> _{pa} (mV)	<i>E</i> _{pc} (mV)	<i>E</i> _{on} (mV)	$\frac{\Delta E_p}{110 \text{ mVs}}$	$\frac{\Delta E_p}{110 \text{ mVs}}$	<i>K</i> ⁰ (cm/s)	<i>A</i> _{eff} (cm ²) 0.10 ⁻²	<i>C</i> _{pseudo} (μF/cm ²)	APW ^a
SWCNT	21.0 ± 0.07	-24.1 ± 0.12	0.87	-161 ± 0.00	-246 ± 0.51	-271 ± 3.20	66.1 ± 1.43	83.6 ± 0.62	0.80 ± 0.00	1.15	54.9 ± 2.40	1.14 ± 0.01
SWCNT/TOCNF-PEI	31.5 ± 1.10	-36.1 ± 2.30	0.87	-167 ± 0.70	-239 ± 0.63	-266 ± 0.21	53.0 ± 1.52	71.5 ± 1.01	4.20 ± 0.40	2.09	52.1 ± 3.01	1.15 ± 0.01

^a APW were defined with the threshold current limits of ±10 μA i.e., ±140 μA/cm², *N* = 3.

a positive charge) and the negatively charged surface of SWCNT. The point of zero charge (pzc) of SWCNT is approximately around 0 V at a pH of ~7. Consequently, at the formal potential of the Ru reaction, it's expected that the surface of SWCNTs would be negatively charged. Thus, the role of nanocellulose would be mainly to increase the access of Ru inside the network by enhancing its wettability. Both electrodes displayed quasi-reversible behaviour with increasing Δ*E*_p as a function of scan rate, as shown in Fig. S4 and summarized in Table 2. The electrochemically active surface area (*A*_{eff}) of the SWCNT and SWCNT/TOCNF-PEI electrodes was studied by using the Randles-Ševčík equation [62]. The *A*_{eff} for SWCNT and SWCNT/TOCNF-PEI was calculated to be 1.147 × 10⁻² cm² and 2.09 × 10⁻² cm², respectively (refer to Fig. S5). These results highlight the potential advantages of integrating TOCNF-PEI into the SWCNT network.

The heterogeneous charge-transfer rate constant (*k*⁰) was determined for both the SWCNT and SWCNT/TOCNF-PEI electrodes using Nicholson's method, considering the values of Δ*E*_p [62]. The close alignment of peak potentials for both electrodes suggests that there was no negative alteration in charge transfer kinetics. Under these conditions, it was assumed that the electronic density of states at the electrode's surface remained consistent for both SWCNT and SWCNT/TOCNF-PEI electrodes. Furthermore, Raman spectroscopy corroborates these findings, demonstrating that the signature of SWCNT remained unchanged following modification with nanocellulose. It's crucial to emphasize that the OSR system operates as a pure electron transport mechanism, intricately linked to the electronic structure of the

working electrode material, rather than its surface chemistry. The analytical potential window (APW) and pseudocapacitance (C_{pseudo}) at SWCNT/TOCNF-PEI and SWCNT electrodes were evaluated and compared in PBS pH 7.4 using CV (refer to Fig. S6, Table S2 and Table 2). C_{pseudo} represents the capacitance resulting from the addition of faradaic components to the true double-layer capacitance [63]. These faradaic reactions at carbon electrodes are mainly attributed to oxygen functionalities on the surface [63]. Additionally, it's probable that metal residues within the structure also play a role in the faradaic reactions, contributing to the measured C_{pseudo} [44,49]. Notably, there were no noticeable differences in APW and C_{pseudo} between SWCNT/TOCNF-PEI and SWCNT electrodes, indicating similar electrochemical behaviour (Table 2).

Fig. 4B presents the electrochemical performance testing of SWCNT and SWCNT/TOCNF-PEI electrodes in $100 \mu\text{mol L}^{-1}$ TC in PBS 7.4, within a potential range of -0.2 V to 1.1 V by using CV. Two anodic oxidation peaks appeared at potentials of 0.65 V and 0.85 V vs. Ag/AgCl, corresponding to the oxidation of TC. Notably, the SWCNT/TOCNF-PEI electrode exhibited a higher oxidation peak current compared to the SWCNT electrode. This enhancement can be attributed to the presence of a hydrophilic layer of TOCNF-PEI on the SWCNT surface, which promotes interactions with TC. As SWCNTs are inherently slightly hydrophobic, the presence of hygroscopic nanocellulose promotes better wetting of the sensor network by the electrolyte solution. Furthermore, TOCNF-PEI carries a positive electrostatic overall charge (Fig. S2), inducing electrostatic attraction toward the partial anionic charge of the zwitterionic TC molecules, yet not completely capturing the TC. These factors facilitate the efficient transfer of charges between TC molecules and the SWCNT/TOCNF-PEI sensor interface, thereby contributing to the observed increase in the oxidation peak current of TC [30,64].

3.3. Optimization of sensor

The effects of various parameters were studied and optimized to enhance the electrochemical behaviour of SWCNT/TOCNF-PEI for TC sensing (as depicted in Table 3). In this study, the impact of different ratios of TOCNF to PEI (3:1, 2:1, 1:1, and 1:2) on the oxidation peak current of $100.0 \mu\text{mol L}^{-1}$ TC in 0.1 mol L^{-1} PBS (pH 7.4) was carefully investigated using DPV. The TOCNF: PEI ratio of 2:1 exhibited superior performance compared to other sample ratios, as illustrated in Fig. 5A. This optimal ratio facilitated an ideal balance between enhancing wetting properties and preserving sufficient surface area of SWCNTs for efficient electron transfer. Increasing the TOCNF content beyond this optimal ratio led to a notable reduction in the signal current, possibly due to the increased density of the TOCNF network acting as a backbone within the TOCNF-PEI layer. The titration measurements indicated that

Table 3

Optimized parameters at SWCNT/TOCNF-PEI for detection of TC.

Optimization parameters	Study target	Optimized results
TOCNF-PEI ratio	wetting behaviour	2:1
Incubation time	TC accumulation	5 min
pH	Signal current and potential	7.4

the charge neutrality in an aqueous TOCNF-PEI complex is obtained already when the mass proportion of the added PEI into TOCNF suspension is only $\sim 6 \text{ w-\%}$ of that of the TOCNF (Fig. S2). This indicates that the overall charge of TOCNF-PEI in all the studied ratios is on the cationic side and, thus probably the sign of charge is not as critical factor differentiating the studied TOCNF-PEI layer compositions as the TOCNF network backbone density, a parameter directly dependent on the mixture component ratio. Nevertheless, the substantial influence of the component ratio on the performance of the sensor underscores the importance of maintaining a delicate balance in the sensor's composition. By ensuring maximal wetting while retaining adequate SWCNT surface area, the optimization strategy effectively enhances overall sensor performance [58]. The influence of different incubation times (0, 5, 10, 15, and 20 min) on the oxidation peak current of $10.0 \mu\text{mol L}^{-1}$ TC in 0.1 mol L^{-1} PBS solution pH 7.4 was studied at SWCNT/TOCNF-PEI (under optimized conditions) by using DPV. The best response signal for the first and second TC oxidation peaks was obtained at 5 min. By increasing time, the current of the response signal decreased slightly and remained steady for 10 min (shown as the second peak in Fig. 5B). The effect of the supporting electrolyte's pH on the oxidation peak current of $100.0 \mu\text{mol L}^{-1}$ TC was studied in a pH range of 3.0–8.0 by using DPV. As protons participate in the oxidation of TC, the oxidation peak current increases from pH 3.0 to 7.4 but decreases at higher pHs due to fewer available protons (Fig. 5C). Similarly, the oxidation peak potential shifted to less positive potentials when pH increased from 3.0 to 8.0 (Fig. 5D). The shift in potential concerning pH value for both peaks demonstrated a direct correlation with pH within the range under examination, as illustrated in Fig. 5D. The obtained slopes of both signals recorded at potentials of 0.65 V and 0.85 V (60.1 mV/pH and 60.08 mV/pH , respectively) were close to the theoretical Nernst value of 59 mV/pH [67]. This observation indicates the participation of an equal number of both protons and electrons during the reaction, as depicted in Scheme S2 [16,68–71]. The optimal signal was obtained at pH 7.4, which is physiologically relevant and similar to the pH of the MBR effluent sample under study. In this work, the optimized parameters were used across all studies (Table 3).

The effect of scan rate (ν) on the I_{pa} of TC signals at the SWCNT/TOCNF-PEI interface was investigated by using CV, as detailed in Fig. 6A and Fig. S7. Notably, I_{pa} displayed enhancement with increasing

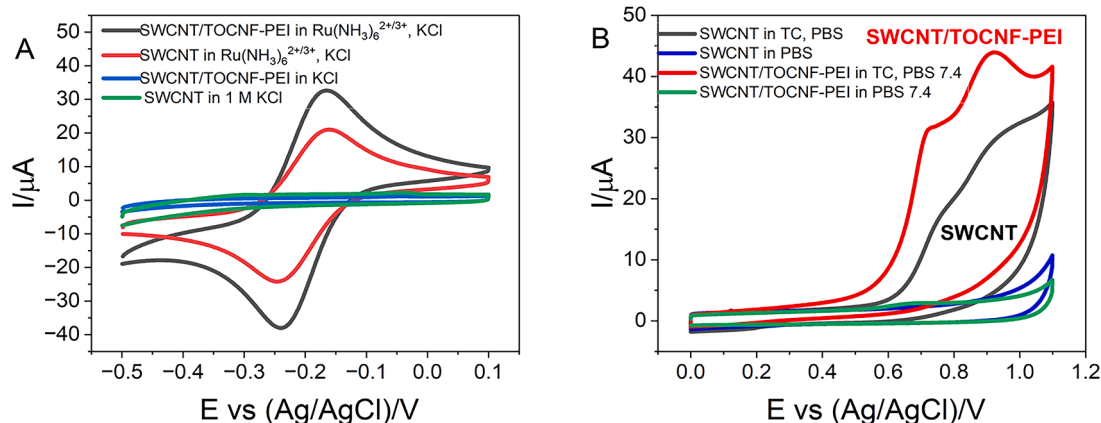


Fig. 4. CVs of SWCNT and the SWCNT/TOCNF-PEI electrodes in 1 mmol L^{-1} $\text{Ru}(\text{NH}_3)_6^{2+/3+}$ in 1 mol L^{-1} KCl (A); and $100 \mu\text{mol L}^{-1}$ TC in 0.1 mol L^{-1} PBS pH 7.4 (B). The scan rate was 0.1 Vs^{-1} .

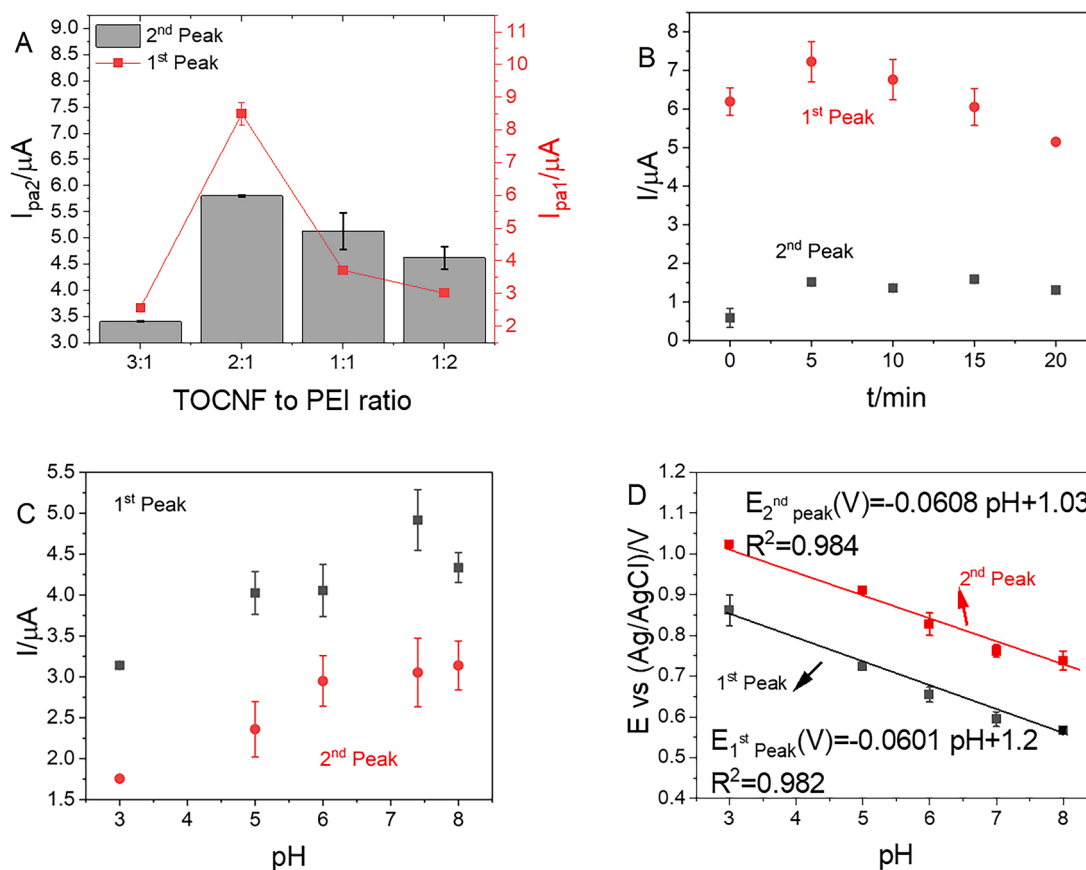


Fig. 5. The effects of TOCNF to PEI ratio (3:1, 2:1, 1:1, 1:2) (A); the incubation time (0, 5, 10, 15 and 20 min) (B); pH on TC oxidation peak current (C); and pH on oxidation peak potential (D), of TC at SWCNT/TOCNF-PEI electrode ($N = 3$).

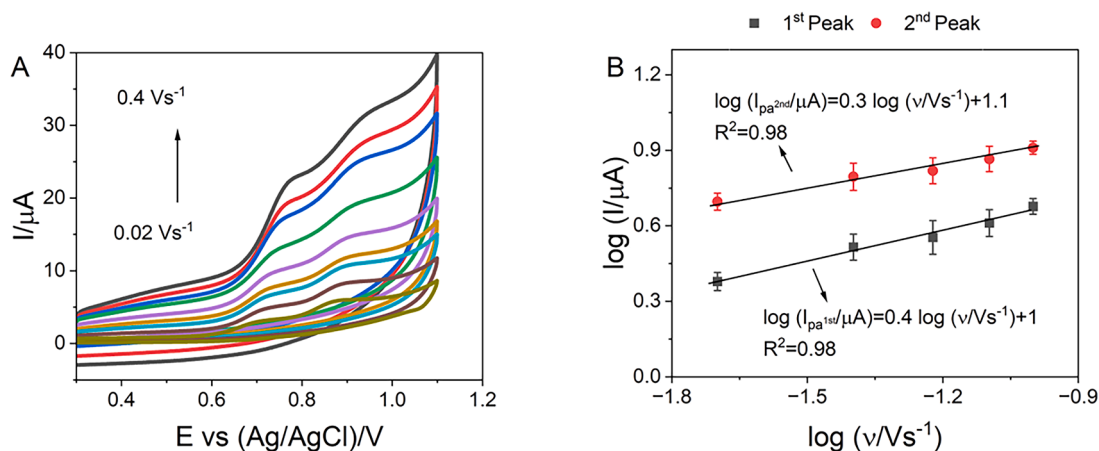


Fig. 6. Cyclic voltammograms of the 100.0 $\mu\text{mol L}^{-1}$ TC in 0.1 mol L^{-1} PBS (pH 7.4) at SWCNT/TOCNF-PEI electrode in various ν (0.02, 0.04, 0.06, 0.1, 0.15, 0.2, 0.3 and 0.4 Vs^{-1}) (A); plot of the logarithm of anodic peak currents vs. logarithm of scan rate with fits of lines for first and second anodic peaks (B).

ν for both peaks. Further analysis involved plotting $\log(I_{pa})$ against $\log(\nu)$ (Fig. 6B), revealing slopes of < 0.5 for both the first (slope of 0.4) and second (slope of 0.3) peaks. This deviation from a slope of 0.5, typical for purely diffusion-controlled processes, suggests the presence of additional factors influencing the electrochemical behaviour. One such factor could be the partial blocking of the electrode surface, resulting in a reduced current compared to what would be expected solely based on diffusion control. This partial blocking effect may be attributed to the presence of nanocellulose, which could hinder the interaction of TC with the available SWCNT surface. Consequently, TC molecules might not be

able to access all binding sites on the electrode surface due to the obstructive influence of nanocellulose.

3.4. Electroanalysis of TC in PBS by DPV

The analytical performance of the SWCNT/TOCNF-PEI electrode was assessed across various TC concentrations, ranging from 0.0 to 125 $\mu\text{mol L}^{-1}$, using DPV under optimized conditions in a 0.1 mol L^{-1} PBS solution at pH 7.4, as shown in Fig. 7A. Notably, the response signal of the SWCNT/TOCNF-PEI electrode exhibited a proportional increase with

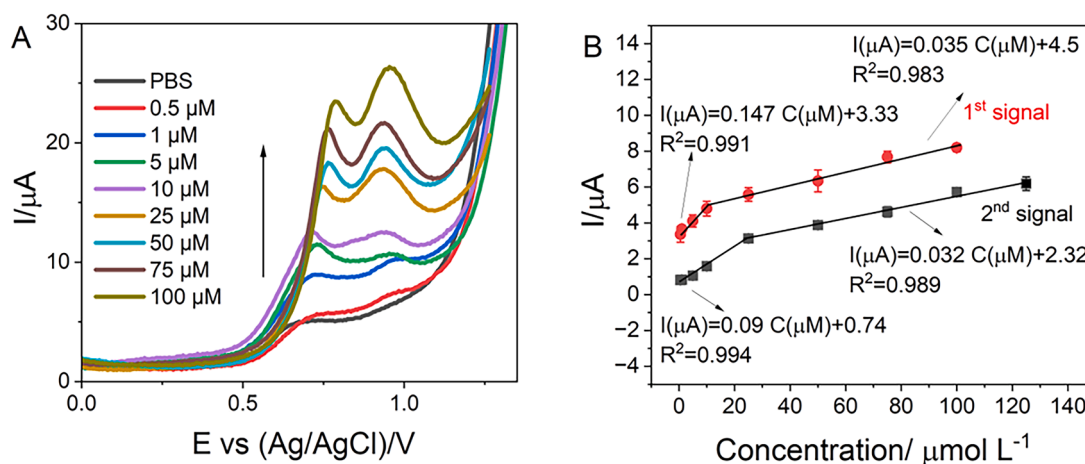


Fig. 7. DPV signals for different concentrations of TC at SWCNT/TOCNF-PEI electrode in 0.1 mol L⁻¹ PBS pH 7.4 (A); the corresponding calibration plot for the SWCNT/TOCNF-PEI electrode ($N = 3$.) (B). The incubation time was 5 min. The pulse time was 0.05 s, the pulse size was 75 mV, and the electrode area was 0.07 cm².

rising TC concentration. The recorded peak currents showed a two-linear relationship with TC concentration within the ranges of 500 nmol L⁻¹ to 25 $\mu\text{mol L}^{-1}$ and 25 $\mu\text{mol L}^{-1}$ to 125 $\mu\text{mol L}^{-1}$ for both signals recorded at potentials of 0.65 V and 0.85 V. Within the concentration range of 500 nmol L⁻¹ to 25 $\mu\text{mol L}^{-1}$, the slope of the linear calibration curve was determined to be 0.09 $\mu\text{A}/\mu\text{mol L}^{-1}$ at a potential of 0.85 V and 0.147 $\mu\text{A}/\mu\text{mol L}^{-1}$ at a potential of 0.65 V. This reduced to 0.032 $\mu\text{A}/\mu\text{mol L}^{-1}$ at a potential of 0.85 V and 0.035 $\mu\text{A}/\mu\text{mol L}^{-1}$ at a potential of 0.65 V in the concentration range of 25 $\mu\text{mol L}^{-1}$ to 125 $\mu\text{mol L}^{-1}$. The observed change in slope in both signals (from 0.147 to 0.035 at a potential of 0.65 V and from 0.09 to 0.032 at a potential of 0.85 V) suggests a transition in the reaction mechanism at a certain concentration threshold of 25 $\mu\text{mol L}^{-1}$. At lower concentrations ranging from 500 nmol L⁻¹ to 25 $\mu\text{mol L}^{-1}$, the response signal was predominantly governed by the adsorption of TC molecules onto the electrode surface, leading to the formation of a sub-monolayer. This adsorption process significantly enhanced the rate of electron transfer, resulting in a steeper slope observed in the calibration curve and higher sensitivity. As the concentration increased beyond 25 $\mu\text{mol L}^{-1}$, the deeper adsorption sites on the electrode surface started to become saturated. This saturation marked a transition toward the establishment of a monolayer-covered surface, where TC molecules continued to adsorb until the surface was fully coated by a monolayer [69]. Consequently, the reaction mechanism shifted to being primarily controlled by diffusion. In this diffusion-limited regime, the rate of mass transport of TC molecules to the electrode surface governs the reaction kinetics, leading to a less steep slope. The high correlation coefficient ($R^2 = 0.99$) of the calibration curve (depicted in Fig. 7B) indicates the robust linear relationship between TC concentration and peak current. The limit of detection (LOD) for both TC oxidation signals was evaluated to be 0.180 $\mu\text{mol L}^{-1}$ at a potential of 0.85 V and 0.112 $\mu\text{mol L}^{-1}$ at a potential of 0.65 V, with a sensitivity of 0.357 $\mu\text{A } \mu\text{mol}^{-1} \text{ L cm}^{-2}$. These findings underscore the remarkable sensitivity and accuracy of the SWCNT/TOCNF-PEI electrode in detecting TC across a broad concentration range, highlighting its promising potential for practical applications in electrochemical sensing.

3.5. Repeatability, reproducibility, and long-term stability studies

We performed additional tests to evaluate the repeatability, reproducibility, and long-term stability of the SWCNT/TOCNF-PEI electrode. Repeatability was assessed by conducting five consecutive measurements of a 50 $\mu\text{mol L}^{-1}$ TC solution using DPV, resulting in an RSD of 3.4% at a potential of 0.65 V and 1.8% at a potential of 0.85 V. Reproducibility was evaluated by fabricating five independent

electrodes and measuring their response to the same TC concentration, yielding an RSD of 3.6% at a potential of 0.65 V and 2.1% at a potential of 0.85 V. Long-term stability was tested by storing the electrode at room temperature and measuring its response periodically over 20 days. The electrode retained 92% of its initial response after 20 days, indicating good stability.

3.6. Interference study

The selectivity and anti-interference ability of the sensor for TC quantification was evaluated by recording the DPV signal of the sensor in response to TC (50 $\mu\text{mol L}^{-1}$) in the presence of two antibiotics (sulfamethoxazole and trimethoprim) to examine their interference with TC quantification. The presence of 1-fold sulfamethoxazole and 50-fold trimethoprim did not significantly affect the DPV signal of TC with a signal change of less than ~10%. In addition, 50-fold urea and 50-fold some common ions, including Na⁺, K⁺, Ca²⁺, Cl⁻, and NO₃⁻ did not interfere with the determination of TC. Thus, the electrochemical sensor is highly resistant to interference, showing a high potential for use in the quantification of TC in real MBR effluent samples.

3.7. Electroanalytical application in MBR effluent sample

The effluent from an MBR has typically undergone extensive treatment, including the removal of suspended solids and various contaminants, making it suitable for discharge into the environment, further treatment, or reuse in certain applications [8,9]. Monitoring and adjusting the properties of the MBR effluent, including factors like pH, nutrient levels, and the concentration of contaminants, is essential to ensure that it meets regulatory standards [14]. In this context, the effectiveness of the SWCNT/TOCNF-PEI electrode in detecting TC in an undiluted MBR effluent sample (pH 7.5) was evaluated using DPV under optimized conditions (Fig. 8A and 8B). The results demonstrated a consistent relationship between the response signal and TC concentration over a range from 0.5 $\mu\text{mol L}^{-1}$ to 75 $\mu\text{mol L}^{-1}$ (Fig. 8C). The LOD was calculated to be 2.46 $\mu\text{mol L}^{-1}$ at a potential of 0.82 V and 1.5 $\mu\text{mol L}^{-1}$ at a potential of 0.65 V, with a sensitivity of 4.55 $\mu\text{A } \mu\text{mol}^{-1} \text{ L cm}^{-2}$. Typically, MBR effluent contains low levels of suspended solids, proteins, carbohydrates, fats, and some pathogens. The slight drop in LOD transitioning from PBS to the MBR environment indicates potential adsorption of these species on SWCNTs, possibly interfering with TC interactions, as evidenced by the calibration plot exhibiting only one slope in MBR. However, these findings highlight the SWCNT/TOCNF-PEI electrode's potential for TC detection within the complex matrix of undiluted and not-filtered MBR effluent, contributing

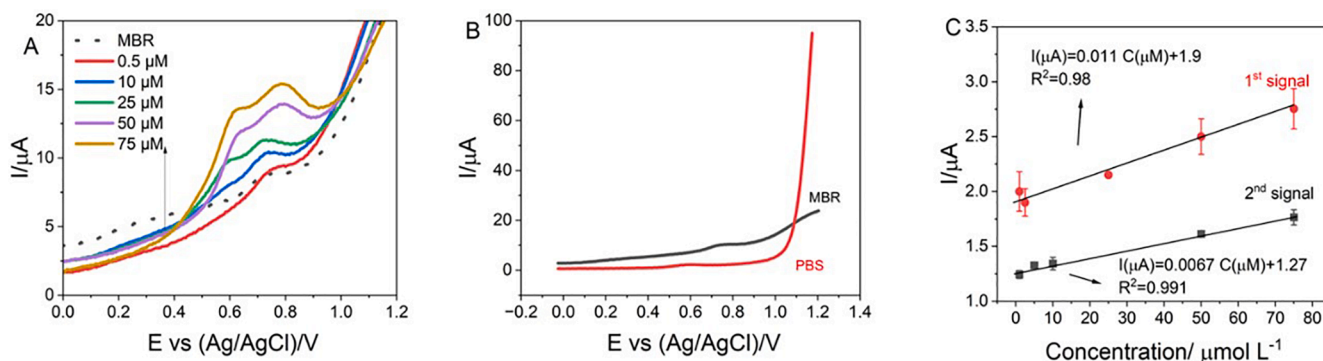


Fig. 8. DPV signals for different concentrations of TC at SWCNT/TOCNF-PEI electrode in MBR (A); DPVs of SWCNT/TOCNF-PEI electrode in MBR and $0.1 \mu\text{mol L}^{-1}$ PBS (pH 7.4) (B); the corresponding calibration plot ($N = 3$) (C). The incubation time was 5 min. The pulse time was 0.05 s, the pulse size was 75 mV, and the electrode area was 0.07 cm^2 .

Table 4

Comparison of the previous TC electrochemical sensors.

sensors	Method		Linear concentration range (mol L^{-1})	LOD (mol L^{-1})	References
PS/CB ^a /GCE ^b	DPV	PBS (pH 7.0)	5.0×10^{-6} – 1.2×10^{-4}	1.15×10^{-6}	[73]
Zr-UiO-66/MWCNTs/AuNPs ^c /GCE	Amperometry	PBS (pH 7.4)	5.0×10^{-7} – 2.25×10^{-4}	1.67×10^{-7}	[17]
PMG ^d /GCE	SWV	PBS (pH 7.4)	5×10^{-6} – 100×10^{-6}	1.6×10^{-6}	[72]
3D-printedGr ^e -PLA ^f	BIA-AD ^g	Acetate buffer (pH 5.0)	5.0×10^{-7} – 50×10^{-6}	1.9×10^{-7}	[18]
PtNPs ^h /C/GCE	CV	PBS (pH 3.0)	9.99×10^{-6} – 4.40×10^{-5}	1st peak: 4.28×10^{-6} 2nd peak: 6.12×10^{-6}	[16]
SWCNT/TOCNF-PEI	DPV	PBS (pH 7.4)	5.0×10^{-7} – 2.5×10^{-5} And 2.5×10^{-5} – 1.25×10^{-4}	1st peak: 1.12×10^{-7} 2nd peak: 1.8×10^{-7} 1st peak: 4.7×10^{-7} 2nd peak: 5.0×10^{-7}	This work

^a Potato starch/carbon black.

^b Glassy carbon electrode.

^c metal-organic framework/multi-carbon nanotubes/gold nanoparticles.

^d Poly (malachite green).

^e Graphite.

^f Polylactic acid.

^g Batch injection analysis with amperometric detection.

^h Platinum nanoparticles supported on carbon.

to the overall quality control and environmental compliance of the treated wastewater in future studies.

The performance of our method was assessed by comparing it with recently published techniques for determining TC. We evaluated their linear dynamic range and limit of detection parameters, and the results are presented in Table 4. The analysis reveals that our method offers a wide linear dynamic range from $0.5 \mu\text{mol L}^{-1}$ to $100 \mu\text{mol L}^{-1}$ in physiologically relevant pH 7.4. This range is the second widest among the methods considered, with the top-ranking method requiring a complicated electrode preparation process [17]. Additionally, our method achieves a commendable detection limit. This performance places it ahead of methods employing hazardous poly (malachite green) [72], costly gold nanoparticles, and MWNT/GO [17]. This makes our method a good choice for environmentally friendly TC detection by utilizing cost-effective cellulose nanomaterials and a simple one-step electrode modification process. The designed SWCNT/TOCNF-PEI offers a practical and attractive solution for TC analysis. It balances performance and sustainability, meeting the rising demand for environmentally conscious analytical methods.

4. Conclusion

In conclusion, our study has successfully developed a multifunctional and sustainable electrochemical sensor based on a novel integration of TOCNFs-PEI with SWCNTs. Through a comprehensive investigation encompassing physicochemical and electrochemical analyses, we have gained valuable insights into the intricate relationships between the

material's properties and its electrochemical performance. Our findings highlight the sensor's remarkable capability to detect TC concentrations across various matrices, including controlled environments and treated wastewater effluents. The achieved limits of detection, particularly in challenging real-world samples, underscore the sensor's sensitivity and applicability in practical scenarios. Moreover, our research emphasizes the scalability and compatibility of the designed cellulose-based sensing architecture with large-scale production. This aspect is pivotal for translating laboratory findings into real-world applications, facilitating the widespread deployment of green and versatile sensing devices. Our study demonstrates the potential of the SWCNT/TOCNF-PEI sensor for the sensitive detection of TC. The sensor's performance in the analysis of untreated and undiluted real MBR effluent samples underscores its practical applicability, making it a promising electrochemical sensor for environmental monitoring and antibiotic detection.

Declaration of generative AI in scientific writing

During the preparation of this work, the author(s) used ChatGPT 3.5 to improve readability and language. After using this tool/service, the author(s) reviewed and edited the content as needed and take(s) full responsibility for the content of the publication.

Supplementary data

Cyclic voltammograms of SWCNT and SWCNT/TOCNF-PEI electrodes in various supporting electrolytes (KCl and PBS) and real sample medium

(MBR effluent); The FTIR spectrum of the SWCNT, the SWCNT/PEI, the SWCNT/TOCNF-PEI and SWCNT/TOCNF. The plot of peak-to-peak separation as a function of scan rate observed in Ru (NH₃)₆^{2+/3+}, KCl solution at SWCNT and SWCNT/TOCNF-PEI electrodes; Scheme of TC Oxidation mechanism; Cyclic voltammograms of the 1 mmol L⁻¹ Ru (NH₃)₆^{2+/3+} in 1 mol L⁻¹ KCl at SWCNT and SWCNT/TOCNF-PEI electrodes in various ν with corresponding plots of the anodic peak currents vs. different $\sqrt{\nu}$ with fits of lines to these data ($N = 3$); Table of relative amounts of the different components of nitrogen, as compared to the total amount of nitrogen in the TOCNF-PEI samples obtained from XPS results; Table of the C_{pseudo} obtained from CV measurements conducted in blank PBS 7.4; Figures related to the study of analytical potential window limit; description and results for TOCNF/PEI charge equilibrium point titration of TOCNF-PEI suspension.

CRedit authorship contribution statement

Khadijeh Nekouei: Writing – review & editing, Writing – original draft, Visualization, Validation, Methodology, Investigation, Formal analysis, Data curation, Conceptualization. **Katri S. Kontturi**: Writing – review & editing, Formal analysis. **Kristoffer Meinander**: Writing – review & editing, Investigation, Formal analysis, Conceptualization. **Ulviyya Quliyeva**: Writing – review & editing, Formal analysis. **Ayesha Kousar**: Writing – review & editing, Formal analysis. **Vasuki Durairaj**: Writing – review & editing, Formal analysis. **Tekla Tammelin**: Writing – review & editing. **Tomi Laurila**: Writing – review & editing, Supervision.

Declaration of competing interest

The authors declare that they have no known competing financial interests or personal relationships that could have appeared to influence the work reported in this paper.

Data availability

Data will be made available on request.

Acknowledgements

The authors acknowledge Canatu Oy for SWCNT samples. The authors acknowledge Miss Ksenija Golovko for MBR effluent samples. This work was supported by funding from the European Union's Horizon2020 research project number 68011531 CONNECT. The authors acknowledge the provision of facilities by the Aalto University Ota Nano–Micronova Nanofabrication centre, OtaNano–Nanoscience centre (Aalto-NMC).

Supplementary materials

Supplementary material associated with this article can be found, in the online version, at [doi:10.1016/j.electacta.2024.144639](https://doi.org/10.1016/j.electacta.2024.144639).

References

- S. Aydin, M.E. Aydin, A. Ulvi, H. Kilic, Antibiotics in hospital effluents: occurrence, contribution to urban wastewater, removal in a wastewater treatment plant, and environmental risk assessment, *Environ. Sci. Pollut. Res. Int.* 26 (2019) 544–558.
- J.L. Martínez, Antibiotics and antibiotic resistance genes in natural environments, *Science* 321 (2008) 365–367.
- Y. Liu, D. Cai, X. Li, Q. Wu, P. Ding, L. Shen, J. Yang, G. Hu, J. Wu, L. Zhang, Occurrence, fate, and risk assessment of antibiotics in typical pharmaceutical manufacturing and receiving water bodies from different regions, *PLoS ONE* 18 (2023) e0270945.
- K.S. Le Corre, C. Ort, D. Kateley, B. Allen, B.I. Escher, J. Keller, Consumption-based approach for assessing the contribution of hospitals towards the load of pharmaceutical residues in municipal wastewater, *Environ. Int.* 45 (2012) 99–111.
- S. Rodriguez-Mozaz, I. Vaz-Moreira, S. Varela Della Giustina, M. Llorca, D. Barceló, S. Schubert, T.U. Berendonk, I. Michael-Kordatou, D. Fatta-Kassinos, J.L. Martinez, C. Elpers, I. Henriques, T. Jaeger, T. Schwartz, E. Paulshus, K. O'Sullivan, K.M. M. Pärnänen, M. Virta, T.T. Do, F. Walsh, C.M. Manaia, Antibiotic residues in final effluents of European wastewater treatment plants and their impact on the aquatic environment, *Environ. Int.* 140 (2020) 105733.
- A. Joss, S. Zabczynski, A. Göbel, B. Hoffmann, D. Löffler, C.S. McArdell, T. A. Ternes, A. Thomsen, H. Siegrist, Biological degradation of pharmaceuticals in municipal wastewater treatment: proposing a classification scheme, *Water Res.* 40 (2006) 1686–1696.
- J. Radjenović, M. Petrović, D. Barceló, Fate and distribution of pharmaceuticals in wastewater and sewage sludge of the conventional activated sludge (CAS) and advanced membrane bioreactor (MBR) treatment, *Water Res.* 43 (2009) 831–841.
- M. Kalli, C. Noutsopoulos, D. Mamais, The fate and occurrence of antibiotic-resistant bacteria and antibiotic resistance genes during advanced wastewater treatment and disinfection: a review, *Water* 15 (2023) 2084.
- S. Wang, X. Ma, Y. Liu, X. Yi, G. Du, J. Li, Fate of antibiotics, antibiotic-resistant bacteria, and cell-free antibiotic-resistant genes in full-scale membrane bioreactor wastewater treatment plants, *Bioresour. Technol.* 302 (2020) 122825.
- F. Chen, J. Ma, Y. Zhu, X. Li, H. Yu, Y. Sun, Biodegradation performance and anti-fouling mechanism of an ICME/electro-biocarriers-MBR system in livestock wastewater (antibiotic-containing) treatment, *J. Hazard. Mater.* 426 (2022) 128064.
- W. Zheng, X. Wen, B. Zhang, Y. Qiu, Selective effect and elimination of antibiotics in membrane bioreactor of urban wastewater treatment plant, *Sci. Total Environ.* 646 (2019) 1293–1303.
- S.W.I.O.o.W. U.S. Environmental Protection Agency, *Wastewater Management Fact Sheet, Membrane Bioreactors*, in: LAST UPDATED ON AUGUST 25 (Ed.), 2007.
- T.U. Rahman, H. Roy, M.R. Islam, M. Tahmid, A. Fariha, A. Mazumder, N. Tasnim, M.N. Pervéz, Y. Cai, V. Naddeo, The advancement in membrane bioreactor (MBR) technology toward sustainable industrial wastewater management, *Membranes* 13 (2023) 181.
- S. Al-Asheh, M. Bagheri, A. Aidan, Membrane bioreactor for wastewater treatment: a review, *Case Stud. Chem. Environ. Eng.* 4 (2021) 100109.
- J. Li, W. Li, K. Liu, Y. Guo, C. Ding, J. Han, P. Li, Global review of macrolide antibiotics in the aquatic environment: sources, occurrence, fate, ecotoxicity, and risk assessment, *J. Hazard. Mater.* 439 (2022) 129628.
- R.T. Kushikawa, M.R. Silva, A.C.D. Angelo, M.F.S. Teixeira, Construction of an electrochemical sensing platform based on platinum nanoparticles supported on carbon for tetracycline determination, *Sens. Actuators B Chem.* 228 (2016) 207–213.
- X. Weng, J. Huang, H. Ye, H. Xu, D. Cai, D. Wang, A high-performance electrochemical sensor for sensitive detection of tetracycline based on a Zr-Uio-66/MWCNTs/AuNPs composite electrode, *Anal. Methods* 14 (2022) 3000–3010.
- C.E.C. Lopes, L.V. de Faria, D.A.G. Araújo, E.M. Richter, T.R.L.C. Paixão, L.M. F. Dantas, R.A.A. Muñoz, I.S. da Silva, Lab-made 3D-printed electrochemical sensors for tetracycline determination, *Talanta* 259 (2023) 124536.
- K. Nekouei, M. Akhondian, N. Wester, T. Laurila, An ultra-sensitive dopamine measurement platform based on molecularly imprinted polymer-carbon hybrid nanomaterials for in vitro use, *Electrochim. Acta* 445 (2023) 142029.
- K. Nekouei, S. Jafari, M. Amiri, M. Sillanpää, Pre-adsorbed methylene blue at carbon-modified TiO₂ electrode: application for lead sensing in water, *IEEE Sens. J.* 18 (2018) 9477–9485.
- J. Kim, S. Yun, Z. Ounaies, Discovery of cellulose as a smart material, *Macromolecules* 39 (2006) 4202–4206.
- H. Cheng, L. Lijie, B. Wang, X. Feng, Z. Mao, G.J. Vancso, X. Sui, Multifaceted applications of cellulosic porous materials in environment, energy, and health, *Prog. Polym. Sci.* 106 (2020) 101253.
- N.O. Gomes, E. Carrilho, S.A.S. Machado, L.F. Sgobbi, Bacterial cellulose-based electrochemical sensing platform: a smart material for miniaturized biosensors, *Electrochim. Acta* 349 (2020) 136341.
- X. Du, Z. Zhang, W. Liu, Y. Deng, Nanocellulose-based conductive materials and their emerging applications in energy devices - a review, *Nano Energy* 35 (2017) 299–320.
- V. Durairaj, T. Liljeström, N. Wester, P. Engelhardt, S. Sainio, B.P. Wilson, P. Li, K. S. Kontturi, T. Tammelin, T. Laurila, J. Koskinen, Role of nanocellulose in tailoring electroanalytical performance of hybrid nanocellulose/multiwalled carbon nanotube electrodes, *Cellulose* 29 (2022) 9217–9233.
- X. Li, L.-Y. Lin, K.-Y. Wang, J. Li, L. Feng, L. Song, X. Liu, J.-H. He, R. Sakthivel, R.-J. Chung, Streptavidin-functionalized-polyethyleneimine/chitosan/HFO2-Pr6O11 nanocomposite using label-free electrochemical immunosensor for detecting the hunger hormone ghrelin, *Compos. Part B Eng.* 224 (2021) 109231.
- M. Rdest, D. Janas, Effective doping of single-walled carbon nanotubes with polyethyleneimine, *Materials* 14 (2021) 65.
- L. Ma, L. Bai, M. Zhao, J. Zhou, Y. Chen, Z. Mu, An electrochemical aptasensor for highly sensitive detection of zearalenone based on PEI-MoS₂-MWCNTs nanocomposite for signal enhancement, *Anal. Chim. Acta* 1060 (2019) 71–78.
- E. Karabulut, L. Wågberg, Design and characterization of cellulose nanofibril-based freestanding films prepared by layer-by-layer deposition technique, *Soft Matter* 7 (2011) 3467–3474.
- R. Hu, H. Gou, Z. Mo, X. Wei, Y. Wang, Highly selective detection of trace Cu²⁺ based on polyethyleneimine-reduced graphene oxide nanocomposite modified glassy carbon electrode, *Ionics* 21 (2015) 3125–3133.

- [31] L. Riva, A. Fiorati, C. Punta, Synthesis and application of cellulose-polyethyleneimine composites and nanocomposites: a concise review, *Materials* 14 (2021) 473.
- [32] Q. Meng, Z. Xue, S. Chen, M. Wu, P. Lu, Smart antimicrobial Pickering emulsion stabilized by pH-responsive cellulose-based nanoparticles, *Int. J. Biol. Macromol.* 233 (2023) 123516.
- [33] M.I. Swasy, B.R. Brummel, C. Narangoda, M.F. Attia, J.M. Hawk, F. Alexis, D. C. Whitehead, Degradation of pesticides using amine-functionalized cellulose nanocrystals, *RSC Adv.* 10 (2020) 44312–44322.
- [34] N. Zhang, G.-L. Zang, C. Shi, H.-Q. Yu, G.-P. Sheng, A novel adsorbent TEMPO-mediated oxidized cellulose nanofibrils modified with PEI: preparation, characterization, and application for Cu(II) removal, *J. Hazard. Mater.* 316 (2016) 11–18.
- [35] L. Riva, N. Pastori, A. Panozzo, M. Antonelli, C. Punta, Nanostructured cellulose-based sorbent materials for water decontamination from organic dyes, *Nanomaterials* 10 (2020) 1570.
- [36] L. Melone, S. Bonafede, D. Tushi, C. Punta, M. Cametti, Dip in colorimetric fluoride sensing by a chemically engineered polymeric cellulose/bPEI conjugate in the solid state, *RSC Adv.* 5 (2015) 83197–83205.
- [37] L. Riva, A. Fiorati, A. Sganappa, L. Melone, C. Punta, M. Cametti, Naked-eye heterogeneous sensing of fluoride ions by Co-polymeric nanosponge systems comprising aromatic-imide-functionalized nanocellulose and branched polyethyleneimine, *Chempluschem* 84 (2019) 1512–1518.
- [38] S. Takahashi, I. Suzuki, T. Sugawara, M. Seno, D. Minaki, J.-I. Anzai, Alizarin red S-confined layer-by-layer films as redox-active coatings on electrodes for the voltammetric determination of L-dopa, *Materials* 10 (2017) 581.
- [39] S. Takahashi, I. Suzuki, T. Ojima, D. Minaki, J.-i. Anzai, Voltammetric response of alizarin red S-confined film-coated electrodes to diol and polyol compounds: use of phenylboronic acid-modified poly(ethyleneimine) as film component, *Sensors* 18 (2018) 317.
- [40] T. Zhang, W. Wang, D. Zhang, X. Zhang, Y. Ma, Y. Zhou, L. Qi, Biotemplated synthesis of gold nanoparticle–bacteria cellulose nanofiber nanocomposites and their application in biosensing, *Adv. Funct. Mater.* 20 (2010) 1152–1160.
- [41] N. Terasawa, High-performance TEMPO-oxidised cellulose nanofibre/PEDOT:PSS/ionic liquid gel actuators, *Sens. Actuators B Chem.* 343 (2021) 130105.
- [42] N. Terasawa, K. Asaka, High-performance cellulose nanofibers, single-walled carbon nanotubes and ionic liquid actuators with a poly(vinylidene fluoride-co-hexafluoropropylene)/ionic liquid gel electrolyte layer, *RSC Adv.* 9 (2019) 8215–8221.
- [43] N. Wester, E. Mynttinen, J. Etula, T. Lilius, E. Kalso, B.F. Mikkladal, Q. Zhang, H. Jiang, S. Sainio, D. Nordlund, E.I. Kauppinen, T. Laurila, J. Koskinen, Single-walled carbon nanotube network electrodes for the detection of fentanyl citrate, *ACS Appl. Nano Mater.* 3 (2020) 1203–1212.
- [44] E. Leppänen, M. Akhondian, S. Sainio, J. Etula, O. Pitkänen, T. Laurila, Structure-property relationships in carbon electrochemistry, *Carbon N Y* 200 (2022) 375–389.
- [45] E. Leppänen, E. Gustafsson, N. Wester, I. Varjos, S. Sainio, T. Laurila, Geometrical and chemical effects on the electrochemistry of single-wall carbon nanotube (SWCNT) network electrodes, *Electrochim. Acta* 466 (2023) 143059.
- [46] A. Kaskela, A.G. Nasibulin, M.Y. Timmermans, B. Aitchison, A. Papadimitratos, Y. Tian, Z. Zhu, H. Jiang, D.P. Brown, A. Zakhidov, E.I. Kauppinen, Aerosol-synthesized SWCNT networks with tunable conductivity and transparency by a dry transfer technique, *Nano. Lett.* 10 (2010) 4349–4355.
- [47] T. Saito, S. Kimura, Y. Nishiyama, A. Isogai, Cellulose nanofibers prepared by TEMPO-mediated oxidation of native cellulose, *Biomacromolecules* 8 (2007) 2485–2491.
- [48] A. Moaisal, A.G. Nasibulin, D.P. Brown, H. Jiang, L. Khriachtchev, E.I. Kauppinen, Single-walled carbon nanotube synthesis using ferrocene and iron pentacarbonyl in a laminar flow reactor, *Chem. Eng. Sci.* 61 (2006) 4393–4402.
- [49] E. Leppänen, S. Sainio, H. Jiang, B. Mikkladal, I. Varjos, T. Laurila, Effect of electrochemical oxidation on physicochemical properties of Fe-containing single-walled carbon nanotubes, *ChemElectroChem* 7 (2020) 4136–4143.
- [50] N. Wester, E. Mynttinen, J. Etula, T. Lilius, E. Kalso, E.I. Kauppinen, T. Laurila, J. Koskinen, Simultaneous detection of morphine and codeine in the presence of ascorbic acid and uric acid and in human plasma at Nafion single-walled carbon nanotube thin-film electrode, *ACS Omega* 4 (2019) 17726–17734.
- [51] S. Manzoor, M. Talib, A.V. Arsenin, V.S. Volkov, P. Mishra, Polyethyleneimine-starch functionalization of single-walled carbon nanotubes for carbon dioxide sensing at room temperature, *ACS Omega* 8 (2023) 893–906.
- [52] M.S. Dresselhaus, G. Dresselhaus, R. Saito, A. Jorio, Raman spectroscopy of carbon nanotubes, *Phys. Rep.* 409 (2005) 47–99.
- [53] A.J. Onyianta, M. Dorris, R.L. Williams, Aqueous morpholine pre-treatment in cellulose nanofibril (CNF) production: comparison with carboxymethylation and TEMPO oxidation pre-treatment methods, *Cellulose* 25 (2018) 1047–1064.
- [54] M. Shimizu, H. Fukuzumi, T. Saito, A. Isogai, Preparation and characterization of TEMPO-oxidized cellulose nanofibrils with ammonium carboxylate groups, *Int. J. Biol. Macromol.* 59 (2013) 99–104.
- [55] H. Qin, Y. Ji, G. Li, X. Xu, C. Zhang, W. Zhong, S. Xu, Y. Yin, J. Song, MicroRNA-29b/graphene oxide–polyethyleneglycol–polyethylenimine complex incorporated within chitosan hydrogel promotes osteogenesis, *Front. Chem.* 10 (2022) 958561.
- [56] L. Melone, B. Rossi, N. Pastori, W. Panzeri, A. Mele, C. Punta, TEMPO-oxidized cellulose cross-linked with branched polyethyleneimine: nanostructured adsorbent sponges for water remediation, *Chempluschem* 80 (2015) 1408–1415.
- [57] X. Jin, Z. Xiang, Q. Liu, Y. Chen, F. Lu, Polyethyleneimine-bacterial cellulose bioadsorbent for effective removal of copper and lead ions from aqueous solution, *Bioresour. Technol.* 244 (2017) 844–849.
- [58] A.H. Nordin, S. Wong, N. Ngadi, M. Mohammad Zainol, N.A.F. Abd Latif, W. Nabgan, Surface functionalization of cellulose with polyethyleneimine and magnetic nanoparticles for efficient removal of anionic dye in wastewater, *J. Environ. Chem. Eng.* 9 (2021) 104639.
- [59] L. Vanzetti, L. Pasquardini, C. Potrich, V. Vaghi, E. Battista, F. Causa, C. Pederzoli, XPS analysis of genomic DNA adsorbed on PEI-modified surfaces, *Surf. Interface Anal.* 48 (2016) 611–615.
- [60] F. Zhao, Z. Yang, Z. Wei, R. Spinney, M. Sillanpää, J. Tang, M. Tam, R. Xiao, Polyethyleneimine-modified chitosan materials for the recovery of La(III) from leachates of bauxite residue, *Chem. Eng. J.* 388 (2020) 124307.
- [61] H. Hantsche, High resolution XPS of organic polymers, the scienta ESCA300 database. By G. Beamson and D. Briggs, Wiley, Chichester 1992, 295 pp., hardcover, £ 65.00, ISBN 0-471-93592-1, *Adv. Mater.* 5 (1993) 778.
- [62] R.S. Nicholson, Some examples of the numerical solution of nonlinear integral equations, *Anal. Chem.* 37 (1965) 667–671.
- [63] Z. Zapata-Benabith, F. Carrasco-Marín, C. Moreno-Castilla, Preparation, surface characteristics, and electrochemical double-layer capacitance of KOH-activated carbon aerogels and their O- and N-doped derivatives, *J. Power Sources* 219 (2012) 80–88.
- [64] F. da Silva Bruckmann, C.E. Schnorr, T. da Rosa Salles, F.B. Nunes, L. Baumann, E. I. Müller, L.F.O. Silva, G.L. Dotto, C.R. Bohn Rhoden, Highly efficient adsorption of tetracycline using chitosan-based magnetic adsorbent, *Polymers* 14 (2022) 4854.
- [65] R.S. Nicholson, Theory and application of cyclic voltammetry for measurement of electrode reaction kinetics, *Anal. Chem.* 37 (1965) 1351–1355.
- [66] Y. Wang, J.G. Limon-Petersen, R.G. Compton, Measurement of the diffusion coefficients of [Ru(NH₃)₆]³⁺ and [Ru(NH₃)₆]²⁺ in aqueous solution using microelectrode double potential step chronoamperometry, *J. Electroanal. Chem.* 652 (2011) 13–17.
- [67] A.J. Bard, L.R. Faulkner, H.S. White, *Electrochemical methods: Fundamentals and Applications*, John Wiley & Sons, 2022.
- [68] W.S. Fernandes-Junior, L.F. Zaccarin, G.G. Oliveira, P.R. de Oliveira, C. Kalinke, J. A. Bonacin, J. Prakash, B.C. Janegitz, Electrochemical sensor based on nanodiamonds and manioc starch for detection of tetracycline, *J. Sens.* 2021 (2021) 6622612.
- [69] H. Filik, A.A. Avan, S. Aydar, D. Ozyurt, B. Demirata, Determination of tetracycline on the surface of a high-performance graphene modified screen-printed carbon electrode in milk and honey samples, *Curr. Nanosci.* 12 (2016) 527–533.
- [70] M. Gashu, B.A. Aragaw, M. Tefera, Voltammetric determination of oxytetracycline in milk and pharmaceuticals samples using polyurea modified glassy carbon electrode, *J. Food Compos. Anal.* 117 (2023) 105128.
- [71] L.V. Faria, A.P. Lima, F.M. Araújo, T.P. Lisboa, M.A.C. Matos, R.A.A. Munoz, R. C. Matos, High-throughput amperometric determination of tetracycline residues in milk and quality control of pharmaceutical formulations: flow-injection versus batch-injection analysis, *Anal. Methods* 11 (2019) 5328–5336.
- [72] M. Turbale, A. Moges, M. Dawit, M. Amare, Adsorptive stripping voltammetric determination of Tetracycline in pharmaceutical capsule formulation using Poly (Malachite green) modified glassy carbon electrode, *Heliyon* 6 (2020) e05782.
- [73] K.P. Delgado, P.A. Raymundo-Pereira, A.M. Campos, O.N. Oliveira Jr., B. C. Janegitz, Ultralow cost electrochemical sensor made of potato starch and carbon black nanoballs to detect tetracycline in waters and milk, *Electroanalysis* 30 (2018) 2153–2159.